OXFORD
SOT | Society of Toxicology
academic.oup.com/toxsci

Toxicological Sciences, 2023, **191(2)**, 343–356
https://doi.org/10.1093/toxsci/kfac139
Advance Access Publication Date: 30 December 2022
Research article

Structure-activity relationship read-across and transcriptomics for branched carboxylic acids

Shengde Wu, Corie Ellison, Jorge Naciff, Michael Karb, Cindy Obringer, Gang Yan, Yuqing Shan, Alex Smith, Xiaohong Wang, George P. Daston*

Global Product Stewardship, The Procter and Gamble Company, Mason, Ohio 45040, USA

*To whom correspondence should be addressed at Global Product Stewardship, The Procter & Gamble Company, 8700 Mason Montgomery Rd., Mason, OH 45040, USA. E-mail: daston.gp@pg.com.
Shengde Wu, Corie Ellison, and Jorge Naciff contributed equally to this study.

Abstract

The purpose of this study was to use chemical similarity evaluations, transcriptional profiling, *in vitro* toxicokinetic data, and physiologically based pharmacokinetic (PBPK) models to support read-across for a series of branched carboxylic acids using valproic acid (VPA), a known developmental toxicant, as a comparator. The chemicals included 2-propylpentanoic acid (VPA), 2-ethylbutanoic acid, 2-ethylhexanoic acid (EHA), 2-methylnonanoic acid, 2-hexyldecanoic acid, 2-propylnonanoic acid (PNA), dipentyl acetic acid or 2-pentylheptanoic acid, octanoic acid (a straight chain alkyl acid), and 2-ethylhexanol. Transcriptomics was evaluated in 4 cell types (A549, HepG2, MCF7, and iCell cardiomyocytes) 6 h after exposure to 3 concentrations of the compounds, using the L1000 platform. The transcriptional profiling data indicate that 2- or 3-carbon alkyl substituents at the alpha position of the carboxylic acid (EHA and PNA) elicit a transcriptional profile similar to the one elicited by VPA. The transcriptional profile is different for the other chemicals tested, which provides support for limiting read-across from VPA to much shorter and longer acids. Molecular docking models for histone deacetylases, the putative target of VPA, provide a possible mechanistic explanation for the activity cliff elucidated by transcriptomics. *In vitro* toxicokinetic data were utilized in a PBPK model to estimate internal dosimetry. The PBPK modeling data show that as the branched chain increases, predicted plasma Cmax decreases. This work demonstrates how transcriptomics and other mode of action-based methods can improve read-across.

Keywords: structure-activity relationship (SAR); read-across; branched-alkyl carboxylic acids; valproic acid; 2-ethylhexanoic acid

Read-across is an old concept that is being increasingly utilized in chemical risk assessment and regulation. The basic premise for read-across is that compounds with similar chemical structure will have the same biological activity either because they interact with the same target or because they are metabolized to a common intermediate that acts as the active compound. Guidance on how to conduct read-across assessments has been published, including the European Chemicals Agency (ECHA)'s read-across assessment framework (RAAF), as well as scholarly publications that propose heuristic rules for identifying and rating the quality of analogs (eg, Blackburn *et al.*, 2011; Wu *et al.*, 2010), and methods to estimate confidence in the assessment (eg, Blackburn and Stuard, 2014). Finding analogs that have similar chemical structure has been facilitated by the creation of large databases such as the US EPA's CompTox Dashboard (https://www.epa.gov/chemical-research/comptox-chemicals-dashboard), which is searchable by chemical structure. The second requirement of read-across—demonstrating that close structural analogs have the same biological activity—is not always easy to fulfill. If the biological activity of an analog is known, then it is possible to use the appropriate biochemical assay to assess affinity for (or activity at) the target. Otherwise, the only way to address the question of biological similarity is to assess activity over a broad biological space.

Global gene expression analysis after a chemical challenge is an approach that provides extremely broad biological coverage. It has been well established that virtually every biological perturbation, including toxic insult, produces characteristic changes in gene expression in responsive cells/tissues, and that these changes are diagnostic of mode of action (Nuwaysir *et al.*, 1999). Cells in culture are also responsive, and gene expression analysis is one of the richest readouts of biological activity from *in vitro* systems. Several groups (eg, De Abrew *et al.*, 2015; Harrill *et al.*, 2021; House *et al.*, 2017) have shown that it is possible to use gene expression analysis to demonstrate comparable biological activity between structurally related compounds and that a reasonably small panel of cell types can cover a broad range of biological space (De Abrew *et al.*, 2016, 2019). This article describes the use of global gene expression analysis to query the extent to which read-across can be used to group branched-chain carboxylic acids.

Valproic acid (VPA) is a widely used anticonvulsant and as a therapy to treat migraine, bipolar disorders, and other psychotic disorders (Johannessen and Johannessen, 2003; Macritchie *et al.*, 2001) but is also a human teratogen (Lammer *et al.*, 1987; Robert *et al.*, 1984), causing spina bifida in about 1% of babies exposed prenatally. VPA also causes neural tube defects and other abnormalities in animal models (Barnes *et al.*, 1996; Massa *et al.*, 2005;

© The Author(s) 2022. Published by Oxford University Press on behalf of the Society of Toxicology. All rights reserved. For permissions, please e-mail: journals.permissions@oup.com

Downloaded from https://academic.oup.com/toxsci/article/191/2/343/6965632 by guest on 24 September 2025

Menegola *et al.*, 1996; Ornoy, 2009). Its isomer, EHA, has also been shown to be developmentally toxic in rodent models (Hendrickx *et al.*, 1993; Pennanen *et al.*, 1992). There is much less data on the developmental toxicity potential of shorter or longer chain-branched carboxylic acids. These other branched acids are used as intermediates in the production of surfactants, lubricants, plastics and other products; therefore, it was of interest to determine whether they have the potential to have VPA-like effects on development. Narotsky *et al.* (1994) tested VPA and a series of shorter and longer branched carboxylic acids in a screening-level developmental toxicity assay (the Chernoff-Kavlock assay) in rats and mice and found that only 2-ethylhexanoic acid and 2-propylhexanoic acid caused valproate-like effects (or any developmental toxicity, for that matter). These results are sufficient to indicate that some analogs of VPA have developmental toxicity potential; however, they provide no information on whether the active compounds act via the same mode of action, nor do they identify the limits of structural similarity beyond which biological activity diverges. In this study, we used transcriptomics to compare biological activity for branched carboxylic acids both shorter and longer than VPA and to infer both modes of action and developmental toxicity potential for these chemicals. We used connectivity mapping (CMap) as a means of comparing gene expression signatures. While it would be possible in a limited comparison like this one to use clustering analyses, we chose to use CMap for 2 reasons: first, it provides a common context for comparing biological similarity with other read-across exercises, and second, it identifies connections with other substances in the database that can provide clues about the mode of action. We also conducted pharmacokinetic modeling to predict systemic levels and external doses of VPA analogs that would be expected to be equivalent to the NOAEL for VPA.

MATERIALS AND METHODS

Chemicals and reagents

The chemicals evaluated in this study were: 2-ethylhexanol (EHO, CAS# 104-76-7), 2-ethylbutanoic acid (EBA, CAS# 88-09-5), 2-ethylhexanoic acid (EHA, CAS# 149-57-5), sodium valproate (VPA, CAS# 1069-66-5 used as the soluble form of VPA), 2-methylnonanoic acid (MNA, CAS# 24323-21-5), 2-hexyldecanoic acid (HDA, CAS# 25354-97-6), octanoic acid (OA, CAS# 124-07-2), dipentyl acetic acid (DPA, CAS# 5422-52-6) or 2-pentylheptanoic acid (PHA, CAS# 5422-52-6), and 2-propylnonanoic acid (PNA, CAS# 65185-82-2). With the exception of the last 2 chemicals, all were purchased from Sigma-Aldrich (St. Louis, Missouri). DPA was purchased from Aurum Pharmatech (Franklin Park, New Jersey), and PNA from ALFA Chemistry (Ronkonkoma, New York). Positive controls for the gene expression studies were trichostatin A (CAS# 58880-19-6) and ciclopirox olamine (CAS# 41621-49-2,) purchased from Calbiochem (Burlington, Massachusetts) and Sigma-Aldrich, respectively. Dimethyl sulfoxide (DMSO, CAS# 67-68-5) was used as the solvent for all chemicals (Sigma-Aldrich, St. Louis, Missouri). Analytical chemistry standards included d_6 VPA (deuterium labeled VPA; Cerilliant, Round Rock, Texas), o-benzylhydroxylamine hydrochloride, and *N*-(3-dimethylaminopropyl)-*N*′-ethylcarbodiimide hydrochloride (Sigma-Aldrich).

Transcriptomic experiments

Four cell types were used for the transcriptomic experiments: MCF-7 (breast epithelial adenocarcinoma), A549 (lung epithelial carcinoma), HepG2 (hepatocellular carcinoma), and iCell cardiomyocytes (derived from induced pluripotent stem cells, FujiFilm Cellular Dynamics, Madison, Wisconsin). Previous work (De Abrew *et al.*, 2019) has shown that these 4 cell types respond to a diverse range of chemicals, including VPA. MCF-7, A549, and HepG2 cells were purchased from American Type Culture Collection (Manassas, Virginia) and grown in phenol red-free DMEM media containing 10% serum (Invitrogen, Carlsbad, California). The iCell cardiomyocytes were grown in a proprietary maintenance medium (FujiFilm Cellular Dynamics, Inc.) for 168 h before chemical treatment. All cell cultures were performed in 96-well plates with 12 vehicle controls on each plate.

Test concentrations of each chemical were selected by determining cytotoxicity in MCF-7 cells to identify a concentration producing no more than 20% cytotoxicity as measured by the 3-(4,5-dimethylthiazol-2-yl)-2,5-diphenyltetrazolium bromide (MTT) assay. The minimally cytotoxic concentration was selected as the highest concentration (D1) to be tested in each of the 4 cell lines. Cells were treated with D1 and two 10× dilutions of D1 (D2 and D3) for a total of 3 concentrations for each chemical for each cell line. The concentrations tested for EHO, EBA, VPA, HDA, PNA, and OA were 0.5, 0.05, and 0.005 mM; and for EHA, MNA, and DPA were 1, 0.1, and 0.01 mM. The transcriptional profile was determined after 6 h of exposure, a timepoint selected in order to obtain a signature related to the direct mechanism of action (De Abrew, *et al.*, 2016; Lamb *et al.*, 2006; Mitsopoulos and Suntres, 2010; Schyman *et al.*, 2019; Zhang *et al.*, 2014).

Gene expression was detected using the L1000 platform (Genometry, Cambridge, Massachusetts), a high-throughput platform that directly measures 978 validated landmark (LM) genes in whole cell lysates. The expression of the remainder of the genome is highly correlated to the LM genes, allowing inference of the expression of the entire genome (Subramanian *et al.*, 2017). These studies were performed in quadruplicates (n = 4) with the exception of OA (n = 3). The gene expression data have been uploaded to the Gene Expression Omnibus.

Transcriptome analysis

Initial L1000 data processing was carried out on quantile-normalized and log2-transformed signals of genes in gct file format. Differential gene expression of LM genes (extracted from the complete gct files) for the tested chemicals were used to generate gene signatures. lmFit and eBayes functions were used to calculate gene-wise test statistics (moderated t-stats, *p* values, and B-stats). Limma topTable function and Benjamini-Hochberg (BH) correction were used to assemble gene lists. The top 50 most up and downregulated genes with the smallest *p* values (the number of genes recommended by the Clue database developers) (https://clue.io/connectopedia/how_to_construct_cmap_queries) induced by each chemical (treatment vs control within each cell line) were selected as gene signatures to query connectivity map (CMap) databases.

CMap analysis using CMap/LINCS database

The Library of Network-Based Cellular Signatures (LINCS) CMap database query site (https://clue.io/query) is a cloud-based software platform for the analysis of data sets generated using L1000 gene expression assays. Its Touchstone version 1.0 is the reference gene expression data set of the L1000 connectivity map consisting of over 1 million gene expression profiles from 8969 well-studied and annotated small-molecule compounds and genetic reagents tested in 9 human cell lines. It was generated by directly measuring the expression signals of 978 LM genes and inferring the expression of 11 350 additional genes. The web app

Downloaded from https://academic.oup.com/toxsci/article/191/2/343/6965632 by guest on 24 September 2025

uses algorithms to compute an enrichment score to compare for the similarity between the input signature and reference signatures in the database (Subramanian *et al.* 2017). Compound similarity was ranked by the CMap connectivity score (ranging from 100 to −100) that corresponds to a portion of reference gene sets with a greater similarity to the perturbagen than the current query. For example, a score of 95 indicates that only 5% of reference gene sets showed stronger connectivity than the current query to the perturbagen. In general, connectivity scores higher than 90 and lower than −90 were considered to be strong scores.

We also compared the signatures for the branched acids with a more limited database consisting of a selection of 319 chemicals tested in up to 22 concentrations, in up to 20 human cell lines, and 2 time points in either triplicates or quadruplicates for a total of 29 521 samples. This data set has overlapped with LINCS but is enriched in chemicals that are relevant for consumer products. Chemicals included in the database include those from De Abrew *et al.* (2016, 2019) and others (listed in Supplementary Table 1). The log2 fold change of each instance (treatment to its related control values) was calculated for each probe and rank ordered to produce the instance CMap rank matrix. To generate signatures for each instance, an FDR < 0.05 cutoff was used to generate up and downregulated signatures. Top 250 probes with the smallest *p* values for up and downregulated genes were selected as signatures if an instance had no probes with FDR < 0.05. A connectivity score for each instance was estimated with a metric based on the Kolmogorov-Smirnov statistic as described previously (Lamb *et al.*, 2006). The average CMap score matrix was then computed to get the CMap score for the same treatment condition (same experiment, concentration, cell line, and time point) and used for CMap analysis. All the computational analyses and graphical visualization (including barview figures) were computed in R software (version 4.0.0, https://cran.r-project.org/) using limma (v3.44.3; Ritchie *et al.*, 2015) packages and Shiny app (Chang *et al.*, 2021).

Plasma protein binding

Plasma protein binding was determined for each chemical using the equilibrium dialysis method. Pooled (N = 5) female Sprague Dawley rat plasma was purchased from BioIVT (Baltimore, Maryland) and thawed on the day of the study (stored at <−70°C until use). Stocks of each test article were prepared at 1000× the desired test concentration in methanol (0.1 M stock for 100 µM dose and 0.01 M stock for 10 µM dose), based on free base molecular weight and compound purity. The test article dose solutions were prepared at a target concentration of 100 µM or 10 µM, in Dulbecco's Phosphate Buffered Saline (DPBS) with calcium and magnesium, resulting in a final methanol concentration of 0.1%. SpectraPor membranes (molecular weight cut off 12–14 000) were wetted in distilled water for 30 min followed by a 15-min equilibration with the study buffer (DPBS+) and were then placed between the 2 chambers of the equilibrium dialysis unit. Chambers were filled with 700 µl of rat plasma or buffer, dosed with the appropriate concentration of test chemical, and rotated at 10 rpm at 37°C for 24 h. Samples were then transferred to a 96-well plate for analytical analysis. Three to five replicates were prepared for each compound, at each concentration.

Hepatic metabolic clearance assay

Dose solutions of the test articles were prepared at 100× the desired test concentration in 50:50 acetonitrile: KHB hepatocyte buffer (BioIVT), based on free base molecular weight and compound purity. The KHB buffer was a custom preparation with no addition of heptanoic acid (further explanation for the custom prep is provided in the Results section). 100× dose solutions were spiked into the test matrices such that the final concentration would be 10 µM. Suspended, pooled (N = 12) female Sprague Dawley rat hepatocytes were purchased from BioIVT (Lot KJZ). Suspended, mixed-gender human hepatocytes (pool of 10 donors) were purchased from BioIVT (Lot DHO). The hepatocytes were thawed, washed in HT thawing buffer (BioIVT), and centrifuged to pellet the cells. The hepatocytes were then resuspended in warm KHB hepatocyte buffer (custom) to a final concentration of 1 000 000 viable cells/ml. Preliminary time course (0–4 h) experiments were performed for each compound to establish optimal assay conditions to ensure linear depletion of parent chemical with respect to incubation time. Once optimal incubation conditions were determined, definitive experiments were performed in triplicate to characterize parent chemical depletion and apparent *in vitro* intrinsic clearance rate. Assays were conducted in discrete wells of a 24-well test plate in a 37°C incubator. The final reaction volume was 400 µl. After a preincubation period of approximately 4 min, the wells were dosed with the 100× dose solution and swirled to mix. At each sampling timepoint, the plate was removed from the incubator, and designated wells were quenched with an equal volume of ice-cold acetonitrile to stop the enzymatic activity. The quenched wells were held at −20°C. At the conclusion of the experiment, samples were centrifuged in Eppendorf tubes at 14 000 rpm for 20 min at 4°C to sediment any precipitation. An aliquot of the supernatant was removed for loss of parent analysis. When using rat hepatocytes, sampling timepoints for VPA and 2-EHA were 0, 5, 10, 20, 30, 60, 120, and 180 min and for 2-PHA and 2-HDA were 0, 2, 4, 8, 10, 15, 20, and 25 min. For human hepatocytes, timepoints were 0, 30, 60, 90, 120, 150, and 180 min for VPA and EHA and 0, 15, 30, 45, 60, 75, 90, and 120 for PHA and HDA. Chemical stability controls for each compound were evaluated in prequenched matrix over the course of the assay. Because glucuronidation is known to be the primary metabolic route for the test chemicals, a positive control assay was conducted using 7-hydroxycoumarin (10 and 100 µM) with the hepatocytes for 30 min. The primary metabolic pathway for 7-hydroxycoumarin is glucuronidation, and therefore, loss of a parent would be attributed to an active glucuronidation pathway. The loss of 7-hydroxycoumarin and the formation of the glucuronide metabolite were monitored using HPLC with a photodiode array detector.

Caco-2 permeability assay

Caco-2 cells (passages 45 and 47), were seeded onto Transwells (BD Falcon, 24 well, 1.0 µm pore size) at a density of 20 100 cells/well and allowed to grow for 21 days in a 37°C incubator. During the growth period, the growth media was exchanged with fresh growth media (DMEM high glucose, with 10% fetal bovine serum, 2.5% HEPES, 1% nonessential amino acids, 1% sodium pyruvate, 1% L-glutamine, and 1% Pen-Strep) every Monday, Wednesday, and Friday. Stocks of test compounds were prepared at 500× the desired test concentration in methanol (5 mM), based on free base molecular weight and compound purity. The dose solutions were prepared at a target concentration of 10 µM, in DPBS with calcium and magnesium. To achieve physiological pH conditions (6.5/7.4) the apical dose solutions were prepared in DPBS that had the pH lowered to 6.5 by adding 4-morpholineethanesulfonic acid (Sigma M1317), while the basolateral dose solutions were prepared in DPBS at pH 7.4. Prior to dosing the test article wells, a trans-epithelial electrical resistance (TEER) measurement was taken, using an Epithelial Voltohmmeter (EVOM2), to monitor

Downloaded from https://academic.oup.com/toxsci/article/191/2/343/6965632 by guest on 24 September 2025

any changes in barrier integrity due to the compound during incubation. Incubations were performed in triplicate (3 wells in the apical to basolateral [A–B] direction and 3 wells in the basolateral to apical [B–A] direction per compound), with test volumes of 0.3 ml in the apical chamber and 1.0 ml in the basolateral chamber. These volumes provide equivalent fluid levels in the 2 chambers, eliminating the potential effects of a pressure gradient. Immediately following dosing of the wells, a 10 µl aliquot was taken from each donor chamber for analytical measurement. The dosed plates were placed in a 37°C incubator on an orbital shaker set at 100 rpm. At each sampling timepoint (15, 30, 60, 120, and 180 min postdose), the plate was removed from the incubator, and a 100 µl aliquot taken from each receiver chamber (apical or basolateral chamber, depending on the direction being tested). The aliquot was immediately replaced by an equal volume of warm bathing buffer (DPBS at pH 6.5 for apical receiver chambers, and DPBS at pH 7.4 for basolateral receiver chambers). At the end of the study, a 10 µl aliquot was taken from each donor chamber and a final TEER measurement was taken.

Chemical analysis

For the hepatic metabolic clearance analyses, concentrations of VPA, EHA, PHA, and HDA in acetonitrile-quenched supernatants were determined by reversed-phase high-performance liquid chromatography/tandem mass spectrometry (HPLC-MS/MS) operating under positive-ion electrospray multiple reaction monitoring (MRM). Acetonitrile-quenched study samples (200 µl) or analytical standards (200 µl) were combined with 12.5 µl of 1 µg/ml stable isotope-labelled internal standard (VPA-d_6), 25 µl of 0.1 M *o*-BHA (derivatizing reagent) and 25 µl of 0.25 M EDC (coupling reagent) to form the benzylhydroxylamine chemical derivative (Zeng and Cao, 2018) of each test compound and the internal standard. Analytical "matrix-matched" standards and quality control samples (QCs) were prepared in blank quenched hepatocyte matrices. HPLC-MS/MS gradient analysis of the *o*-BHA derivatives was performed on a Sciex 6500+ MS, using a Waters Atlantis dC18 column (3 µM, 2.1 mm × 50 mm) with 0.1% formic acid in water and 0.1% formic acid in acetonitrile as mobile phases. Caco-2 and plasma protein binding analyses were done by electron ionization (EI) GC-MS/MS, using an Agilent 7010B GC-MS with an Agilent DB-5MS 30 m × 0.25 mm × 0.25 µM column. A Restek low-pressure drop liner with wool was used. The Caco-2 sample preparation involved diluting samples 1:9 (v: v) with 200 ng/ml VPA-d_6 in acetonitrile containing 0.1% formic acid, filtering samples on an AcroPrep™ 0.45 µM filter plate (Pall part # 5054), and transferring the filtrate for GC-MS/MS analysis. For the protein binding of HDA, a liquid/liquid extraction method was done by salting out into acetonitrile using a saturated ammonium sulfate solution. Four hundred microliter of rat plasma or buffer was combined with 10 µl of a PHA internal standard solution and 400 µl of acetonitrile, followed by vigorous mixing for 15 min. Four hundred microliter of a saturated ammonium sulfate solution was then added, followed by mixing and centrifugation. The acetonitrile (top) layer was transferred to autosampler vials for analysis by GC-MS/MS.

Permeability, plasma protein binding, and hepatic metabolic clearance data analysis

The percent fraction unbound (Fu) is calculated as F/F + B × 100, where the compound in the donor chamber (DPBS+) is free (F) while the compound in the receiver chamber (plasma) is a mix of free and bound (F + B) compound at the end of the incubation. The % Fu was calculated for each replicate and was then averaged for the compound Fu. Any chambers that exhibited leakiness (plasma crossing into the donor chamber) were excluded from the calculations.

In vitro intrinsic clearance (CLint) and half-life (T1/2) values for test article disappearance were determined using a method described by Obach (1999). Briefly, parent substrate concentrations at each timepoint were normalized to the value obtained at time zero. The natural log of the percentage remaining versus time at each substrate concentration was used to calculate the first-order elimination rate constant (kelm). In cases where the natural log of the substrate remaining versus time plots were nonlinear, only those timepoints where linearity was observed were used to determine elimination rate constants. *In vitro* CLint (Equation 1) and T1/2 (Equation 2) were calculated from the slope of the natural logarithm of the substrate concentration versus time curve, where the slope equals the first-order elimination rate constant, kelm (min-1).

$$\text{Equation 1: } \textit{In vitro } CL_{int} = \left(k(\text{min}^{-1})\right) * \left(\frac{\text{RxVol.}(\mu L)}{\text{mg_protein}}\right)$$

where, k = first-order elimination rate constant (kelm), RxVol. = incubation volume and mg_protein = total amount of protein in each reaction

$$\text{Equation 2: } = t_{1/2} = \frac{\ln 2}{k(\text{min}^{-1})}$$

where, k = first-order elimination rate constant (kelm).

For Caco-2 assays, the apparent *in vitro* permeability constants (cm/min) were calculated with the equation, permeability constant = $S/[AC_0]$, where S is the slope (units of ng/min), A is the cross-sectional area of the tissue surface exposed to solute transport in cm^2 (0.3 cm^2 for Transwells), and C_0 is the initial concentration of solute in the donor chamber in ng/ml.

Bottom-up PBPK modeling approach

It was desirable to have a consistent PBPK modeling approach across the chemicals, and since not all the chemicals had an existing rat *in vivo* PK data for model optimization, it was necessary to utilize a bottom-up PBPK modeling approach (ie, only *in vitro* and *in silico* data are used as model inputs). The model for VPA was used as the representative model to evaluate the bottom-up approach for the current class of chemicals since VPA has existing *in vivo* PK data.

All PBPK model simulations were performed using GastroPlus 9.7 simulation software (Simulation Plus) with the additional ADMET Predictor module. All PBPK model simulations were conducted using the physiology of a 0.25 kg rat as described by GastroPlus (Supplementary Table 1 and Supplementary Figure 2). A fasted gut physiology was used for the advance compartmental absorption and transit model. Metabolism was confined to the liver compartment. All tissues were perfusion limited and other available options within GastroPlus were left at the default settings. Although there is knowledge that VPA undergoes enterohepatic recirculation (Ogiso *et al.*, 1986; Pollack and Brouwer, 1991), this pathway was purposely omitted from the model structure since knowledge of this pathway requires extensive *in vivo* PK data which are not available for the other case study chemicals. Additionally, the relevant dose metric for VPA toxicity is Cmax (Nau, 1986), which would not be impacted by enterohepatic recirculation.

Downloaded from https://academic.oup.com/toxsci/article/191/2/343/6965632 by guest on 24 September 2025

Local sensitivity analysis was utilized to identify when *in vitro* data should be used as input parameters for the PBPK model instead of *in silico* estimates. To accomplish this, the VPA PBPK model was initially parameterized with all *in silico* estimates from ADMET Predictor, except for hepatic metabolism which was estimated from *in vitro* studies as described in the methods. *In vitro* data were used for metabolism estimates since there is currently no reliable way of predicting an *in silico* metabolism rate. A local sensitivity analysis was then performed on this VPA model. The relative influence of each parameter in the model on plasma AUC and Cmax was determined based on the calculated sensitivity coefficients. The sensitivity coefficient was calculated as previously described (Ellison and Wu 2020; Yoon *et al.*, 2009) and is defined as the percent change in the dose metric of interest (plasma AUC or Cmax) resulting from a change in a particular parameter. All model parameters were subject to the sensitivity analysis and a 1% increase and decrease in parameter value relative to baseline was done for a 24 h simulation exposure and an oral dose of 25 mg. A 1% change in parameter was utilized to ensure the model stayed in the region of biologically plausibility for the parameter. Each model parameter was categorized as having low, medium, or high influence on plasma AUC or Cmax using previously reported criteria (International Programme on Chemical Safety (IPCS), 2010).

Final PBPK models for VPA, EHA, PHA, and HDA were initially parameterized with all *in silico* estimates from ADMET Predictor. *In silico* estimates were replaced with *in vitro* data for chemical parameters that were identified as having medium or high sensitivity in the local sensitivity analysis (plasma protein binding, Caco-2 permeability, and hepatic metabolism).

In vitro permeability measured in Caco-2 cell monolayers was scaled to effective *in vivo* oral permeability (Peff) using a log-linear fit to lab-specific Caco-2 apparent permeability (Papp) of reference compounds and their associated Peff values measured via Loc-I-Gut (Lennernäs, 2007). The general equation used for this conversion was: $\text{Peff} = a * \text{Papp} + b$, where the terms a and b were 0.0005843 and 0.06216, respectively.

Partition coefficient values were estimated using the default methods in GastroPlus (Lukacova [Rodgers-Single] for perfusion-limited tissues). *In vitro* metabolism data from hepatocytes was scaled from *in vitro* hepatocyte intrinsic clearance to *in vivo* liver intrinsic clearance using the following equation:

$$\text{CL}_{\text{int}}^{\text{Liver}} = (\text{Compound intrinsic clearance [}\mu\text{l/min/million cells]}) \times (\text{hepatocyte number [cells/g of liver]}) \times (\text{Liver weight[g]})$$

The scaling factors used were a hepatocyte number of 120 million cells/g liver (Barter *et al.*, 2007) and a liver weight of 11 g (GastroPlus physiology). Renal clearance was described as, CLrenal (L/h) = glomerular filtration rate (GFR) * fraction unbound to plasma. The GFR predicted by GastroPlus was 0.078 L/h and the fraction unbound to plasma was the chemical-specific value from *in vitro* studies.

For HDA, there was a minor deviation from the model parameterization workflow described above. A reliable determination of Caco-2 permeability was not achievable due to nonspecific binding during the *in vitro* assay. As such, it was necessary to use a different approach for estimating the input value for this parameter into the PBPK model. First, an *in silico* estimate for the parameter was obtained. The *in silico* value was not used directly in the PBPK model because it was noticed during the parameterization of the other PBPK models (ie, VPA, EHA, and PHA) that the *in silico* values did not always agree with the *in vitro* measure. The data from VPA, EHA, and PHA were used to account for the average fold difference between *in silico* prediction and *in vitro* measure. There was an average of 0.75-fold over prediction for *in silico* predictions for Peff. This correction factor was applied to the *in silico* prediction for HDA and the adjusted value was used in the PBPK model.

A chemical-specific literature review was conducted to locate existing rat plasma PK data following oral exposure that could be used for PBPK model evaluation. Graphs containing plasma concentration data were digitized using GetData graph digitizer (http://getdata-graph-digitizer.com/). The AUC and Cmax of the digitized data were determined using GastroPlus 9.0 (Simulations Plus). To evaluate a given PBPK model, simulations were conducted where all chemical-specific input parameters were held constant to what was described in the previous sections of the methods and only the dosing conditions were modified to reflect the dosing conditions specific for a given PK study. As a simplification, all model simulations used the 0.25 kg rat physiology described earlier in the paper irrespective of the rat strain or bodyweight for a specific PK study. Dosing conditions (amount, frequency, and route) were specific for a given PK study but dose volume, precipitation time, and particle density were left at the default settings in GastroPlus and held constant between simulations. Model estimates for AUC, Cmax, and plasma versus time profile were recorded. Model simulations were compared to the experimental data to determine the AUC and Cmax ratios.

Oral equivalent doses were estimated for VPA, EHA, PHA, and HDA. The PBPK model for VPA was used to estimate the Cmax in plasma, the relevant dose metric for toxicity (Nau, 1986), associated with the oral NOAEL (150 mg/kg). The resulting Cmax in plasma was then set as the target internal exposure metric for EHA, PHA, and HDA, and the corresponding PBPK models were used to determine the oral dose that results in the target Cmax.

Molecular docking

Although many modes of action have been suggested for VPA, our CMap analysis indicated that it is connected most avidly to histone deacetylase (HDAC) inhibitors. Therefore, we undertook a molecular docking exercise to determine whether the degree of affinity for the active site correlates with the transcriptomics results. There are numerous HDAC isoforms; for simplicity, we chose HDACs 1, 3, and 8 as these are all inhibited by the top CMap connecting compounds in the Clue database. The ligand was built by ChemDraw Professional version 20.1.0.110 (PerkinElmer; Akron, Ohio) and prepared for docking using the Schrödinger LigPrep tool. The 2D structures were converted to low-energy 3D structures through the following steps in LigPrep: (1) Adding H atoms and generating a reasonable ionization state at pH = 7.0 ± 2.0 using Schrödinger Epik; (2) Generating all combinations of stereoisomers.

HDAC protein sequences were downloaded from Protein Data Bank (PDB) (PDB ID: HDAC1: 5ICN; HDAC3: 4A69; HDAC8: 5DC5) and were prepared using Schrödinger Protein Preparation Wizard. The protein crystal structures from PDB were converted to full 3D structures for docking calculation through the following steps (1) adding H atoms, assigning correct bond orders, and filling missing side chains and loops using Prime; (2) generating a reasonable ionization state at pH = 7.0 ± 2.0 using Schrödinger Epik; (3) removing unnecessary water molecules and extra protein chains; (4) refining H-bonding by adjusting water orientations and side chain ionization state (using PROPKA pH: 7.0); (5) restraining minimization using force field OPLS_2005. The

Downloaded from https://academic.oup.com/toxsci/article/191/2/343/6965632 by guest on 24 September 2025

receptor grid of each protein was generated using Schrödinger receptor grid generation tool. The original ligand was selected as the center of the receptor site. Zinc ion (Zn^{2+}) was selected as a H-bond/metal constraint. Other settings were used as default. The molecular docking procedure was performed using Schrödinger Glide docking program. Standard precision (SP) and default settings were selected. H-bond/metal constraint (Zn^{2+}) was selected as a constraint to capture the ligand-Zn^{2+} interactions. The results were visualized in Schrödinger Maestro version 12.3.013 (Schrödinger; New York, New York).

RESULTS

Transcriptional profiling and molecular docking

All chemicals produced changes in gene expression in at least 1 of the 4 cell types, with most chemicals producing significant effects in all 4 at the highest dose tested. VPA was the most active of the chemicals evaluated in terms of number of genes affected, with EHA second. EHO is known to be metabolized to EHA but the number of significant gene expression changes elicited by EHO was less than for EHA. The difference could be due to the relatively short time of exposure and the relative limited metabolic capability of the cells evaluated resulting in limited oxidation of the alcohol to EHA.

The high concentration of each chemical elicited the most robust transcriptional changes; therefore, the signatures generated from these concentrations were used for cross-chemical comparisons. We used CMap to determine the degree of similarity of transcriptional profiles as a measure of comparable biological activity. Figure 1 provides a comparison of the connectivity scores for each chemical versus VPA. The gene expression ranks for VPA and EHA are highly correlated with connectivity scores of greater than 90 (out of 100) for every cell type. The correlation between PNA and VPA is also highly positive (again, greater than 90), although not quite as high as the correlation between VPA and EHA. Connections between VPA and the other test chemicals is less strong, with many instances being either not correlated or negatively correlated with the VPA gene expression profile.

The transcriptional signatures for each chemical were evaluated for connections in a large CMap database (https://clue.io/touchstone). It has been demonstrated that this approach is useful to identify chemicals with similar mode of action, regardless of physicochemical properties similarities among the chemicals' signatures being compared (De Abrew *et al.*, 2016, 2019; Lamb *et al.*, 2006). The CMap results (Figure 2) indicate that VPA, EHA, and PNA connect with histone deacetylase (HDAC) inhibitors such as entinostat, droxinostat, apicidin, pyrroxamide, and others. None of the other chemicals in our test set connected with HDAC inhibitors.

Having this insight into the mode of action of these branched carboxylic acids allowed us to use a molecular docking model as an additional means of understanding the gene expression results and in providing more support for considering VPA to be a suitable analog for some of the acids but not others. Binding patterns were similar for the different HDAC subtypes (HDAC1, 3, and 8), so we only show the results for HDAC3 (Figure 3). The results revealed 2 key points: (1) The acid group plays an important role on the salt bridge interaction and coordination with Zn^{2+} as well as H-bonding interaction with His134 and Tyr298 (Figure 3B); (2) the 2 alkyl chains of acids (R and R_1, Figure 3A)

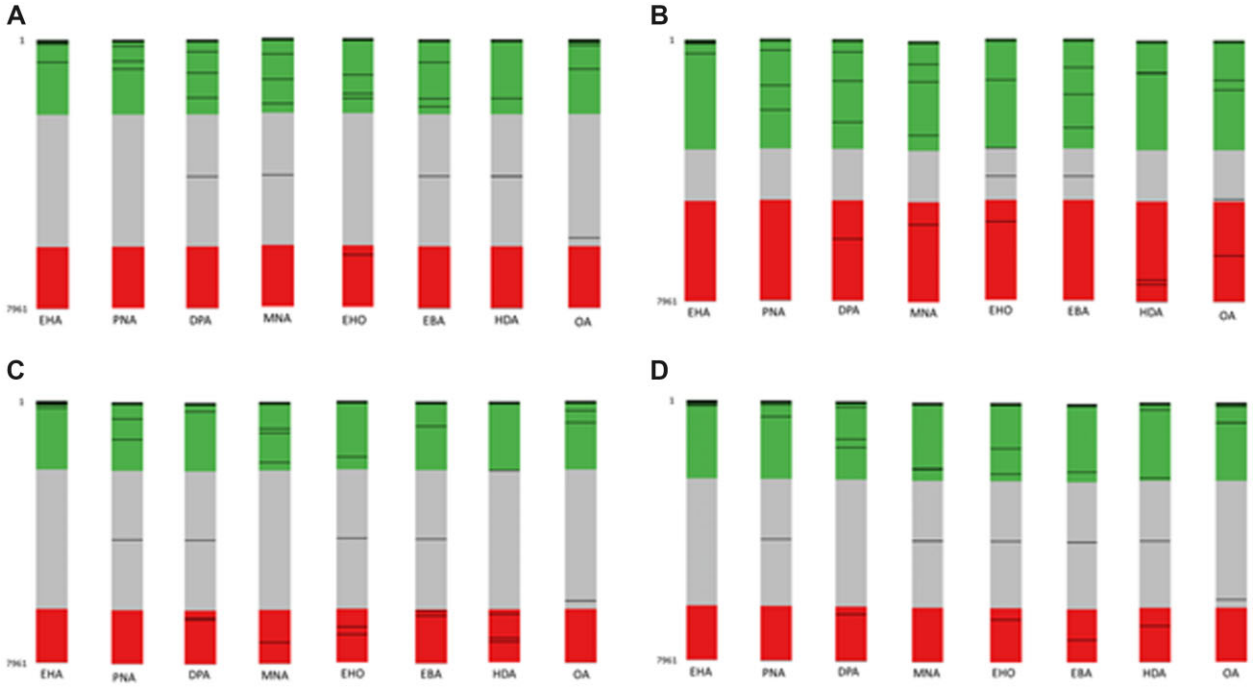

Figure 1. Connectivity mapping of branched carboxylic acids. Signatures of 500μM of VPA tested in 4 cell types were used to query our internal CMap database. A, HepG2, B, MCF7, C, A549, and D, iPS-derived cardiomyocytes. The mapping was done using a database of over 300 chemicals, each of which was tested at multiple concentrations and in different cell types, with 7961 unique combinations of chemical/concentration/cell type, which we call "instances." Each instance was compared with the gene expression signature for VPA. The individual barviews are constructed from these 7961 comparisons, with the instance with the highest CMap score at the top of the barview (ranked number 1) and the instance with the lowest score at the bottom (ranked number 7961). Each black line in a barview represents the relative rank of each cell type/concentration for the indicated chemical as compared to VPA. Instances in the upper (green) part of the bar indicate positive correlation, the lower (red) part negative correlation, and the middle (gray) part, no correlation. The CMap scores for EHA and PNA are high, with most or all treatments in the upper part of the bargraph.

Downloaded from https://academic.oup.com/toxsci/article/191/2/343/6965632 by guest on 24 September 2025

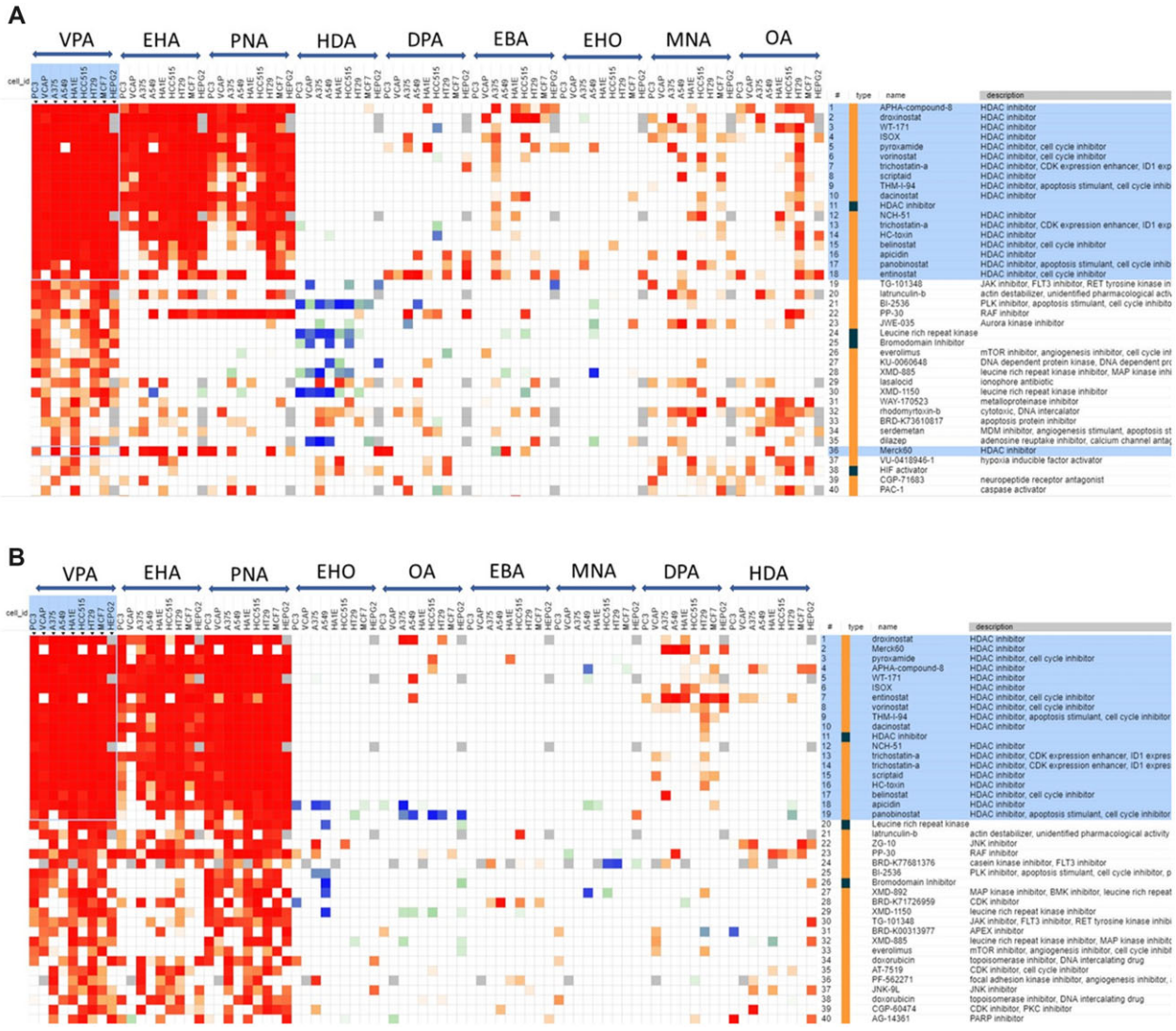

Figure 2. Touchstone heatmaps of CMap analysis using VPA 500 μM signatures (top 50 up and downregulated genes) generated from (A) MCF-7 cells, (B) iCell cardiomyocytes, (C) HepG2 cells, or (D) A549 cells (see Methods section for details). Red indicates strong positive correlation with the treatment or mode of action listed in the column at right, blue indicates a negative correlation, with different color shades indicating the strength of correlation. The top 40 ranked connections are shown. The same compound may be listed multiple times (ie, trichostatin-a), since the individual transcript profile was obtained in different cell types and/or concentrations. VPA, PNA, and EHA connect to HDAC inhibitors; the other chemicals in the test set do not.

interact with the hydrophobic pocket through Van der Waals force. A good HDAC3 ligand must have the right orientation for the acid group to bind with Zn^{2+}, and also have certain chain lengths of R and R_1 to generate sufficient Van der Waals force and also fit well with binding pocket. The docking results show that VPA, EHA, and PNA fit well in the binding pocket of HDAC3 and have good binding via a C2-C3 R group as well as a $C \geq 3$ R_1 group (Figure 3C). However, PHA, HDA, EBA, MNA, and OA did not have good binding due to different reasons. PHA and HDA have oversized alkyl chain R groups ($R \geq C5$) that are too bulky to fit the binding pocket (Figure 3D). EBA, PNA, and OA have either very small R and R_1 groups (EBA) or short R_1 group ($R_1 < C2$ in PNA and OA), which are too small to generate sufficient interactions with the pocket as shown in Figures 3E and 3F, respectively. These results further support the CMap results showing that 3 of the branched carboxylic acids (VPA, EHA, and PNA) have strong connection to HDAC inhibitor but the others do not.

To further confirm the docking results, we applied the model to 10 known HDAC inhibitors related to VPA with teratogenicity data (Eikel *et al.*, 2006). The docking results are consistent with regard to the role of alkyl chain length, position of unsaturated bonds and enantiomeric effects, and teratogenic potential is associated with HDAC inhibition.

Permeability, plasma protein binding, and hepatic metabolic clearance data

The Caco-2 permeability constants, fraction unbound to plasma protein and hepatic metabolic clearance were conducted on 4 of the test chemicals and the results are summarized in Table 1. The permeability constants for VPA, EHA, and PHA indicate that these materials would likely be highly absorbed through the intestinal wall. No permeability data could be generated for HDA due to high nonspecific binding in the test wells and/or cells. HDA exhibited the greatest amount of binding to rat plasma protein, with fraction unbound values of 0.13 and 0.02 for 10 μM and 100 μM, respectively. The extent of plasma protein binding was similar between VPA and EHA and between PHA and HDA. Saturation of protein binding potentially occurred for VPA and

Downloaded from https://academic.oup.com/toxsci/article/191/2/343/6965632 by guest on 24 September 2025

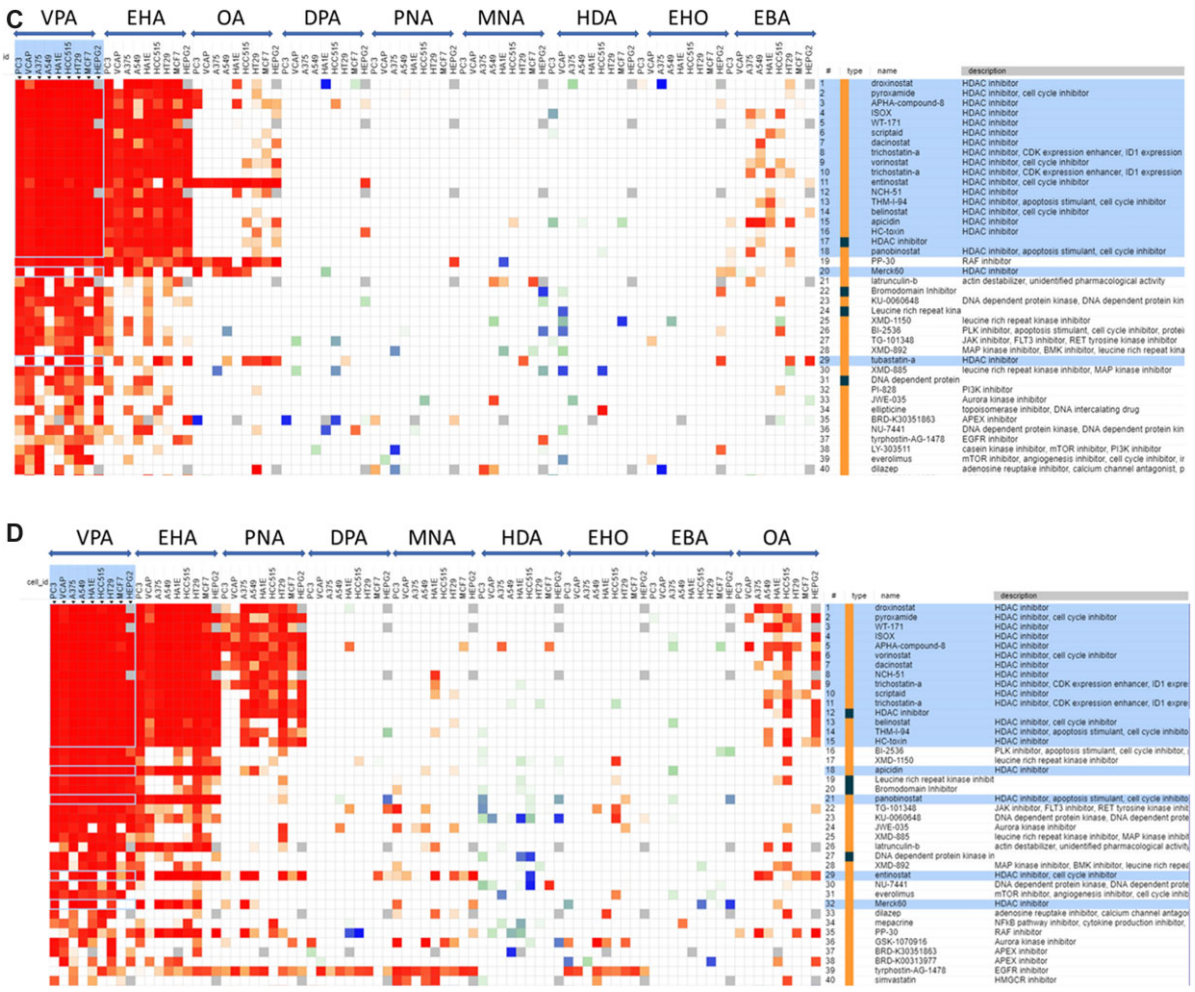

Figure 2. (continued).

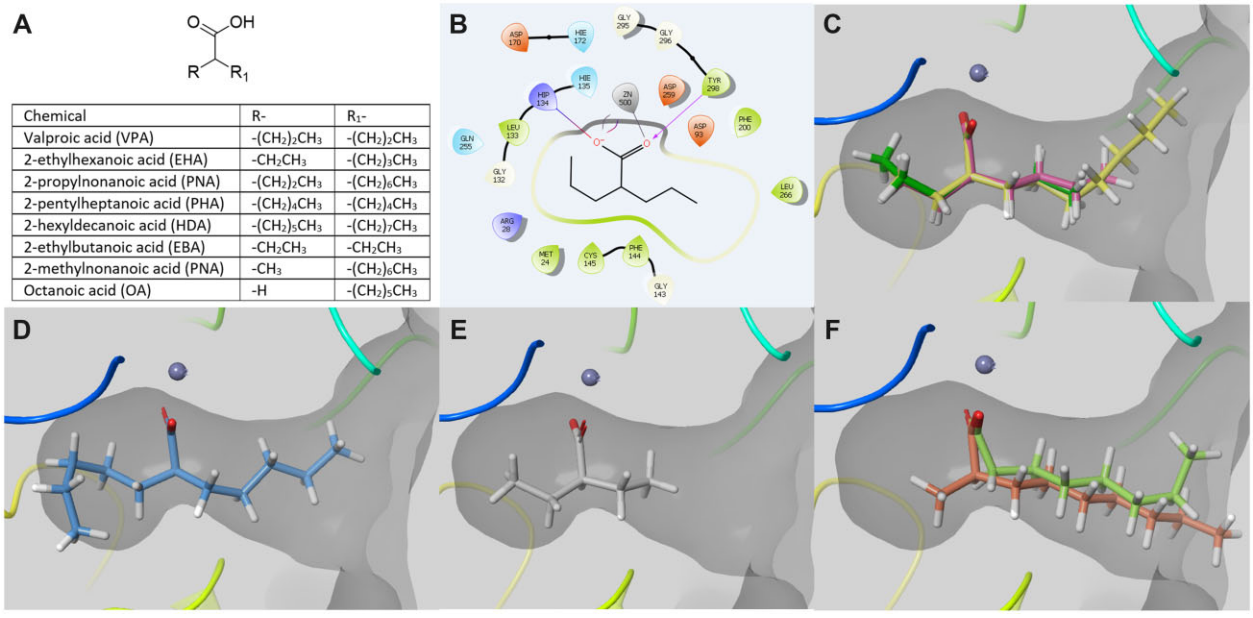

Chemical	R-	R_1-
Valproic acid (VPA)	$-(CH_2)_2CH_3$	$-(CH_2)_2CH_3$
2-ethylhexanoic acid (EHA)	$-CH_2CH_3$	$-(CH_2)_3CH_3$
2-propylnonanoic acid (PNA)	$-(CH_2)_2CH_3$	$-(CH_2)_6CH_3$
2-pentylheptanoic acid (PHA)	$-(CH_2)_4CH_3$	$-(CH_2)_4CH_3$
2-hexyldecanoic acid (HDA)	$-(CH_2)_5CH_3$	$-(CH_2)_7CH_3$
2-ethylbutanoic acid (EBA)	$-CH_2CH_3$	$-CH_2CH_3$
2-methylnonanoic acid (PNA)	$-CH_3$	$-(CH_2)_6CH_3$
Octanoic acid (OA)	-H	$-(CH_2)_5CH_3$

Figure 3. Docking results of different branched alkyl acids against HDAC3. A, Structures of branched fatty acids; B, ligand interaction diagram of VPA; C, binding poses of VPA (green), EHA (pink) and PNA (yellow) (binding pocket is shown as shaded area); D, binding pose of PHA (blue) where a few atoms are outside the binding pocket; due to a very bulky R group, HDA has no reasonable conformation; E, binding pose of EBA (gray); F, binding poses of PNA (orange), and OA (light green).

Downloaded from https://academic.oup.com/toxsci/article/191/2/343/6965632 by guest on 24 September 2025

Table 1. Summary of *in vitro* permeability, plasma protein binding, and hepatocyte metabolism for VPA, EHA, PHA, and HDA

Chemical	Caco-2 Permeability		Fraction Unbound to Rat Plasma Protein		Hepatocyte Metabolism (μl/min/million cells)	
	Rate ($\times 10^{-4}$ cm/min)	permeability class	10 μM	100 μM	Rat	Human
VPA	20.5 ± 3.4	High	0.45 ± 0.02	0.62 ± 0.07	5.4 ± 0.23	~0
EHA	32.3 ± 2.2	High	0.42 ± 0.02	0.54 ± 0.02	12.5 ± 0.40	1.9 ± 0.49
PHA	26.5 ± 5.6	High	0.19 ± 0.04	0.13 ± 0.04	49.6 ± 4.89	23.9 ± 0.66
HDA	N/A	N/A	0.13 ± 0.005[a]	0.02 ± 0.006[a]	89.3 ± 8.79	52.2 ± 1.47

Values are mean ± SD. Caco-2 class based on following criteria: Low, $< 1.2 \times 10^{-4}$ cm/min; Medium, 1.2–12 $\times 10^{-4}$ cm/min; High, $> 12 \times 10^{-4}$ cm/min.
N/A, not available.
[a] Some of the measured values on the buffer sides of the chamber were below the limit of quantitation (1 μM) and were set equal to the LoQ for the calculation of fraction unbound to plasma protein.

EHA since a higher fraction was unbound at the 100 μM test concentration compared to the 10 μM concentration.

Results (data not shown) from the initial rat hepatocyte metabolism studies for VPA and EHA indicated that the chemicals were stable during the 2-h incubation, an unexpected finding since both chemicals have previously been shown to metabolize quickly *in vitro* (Hamdoune *et al.*, 1995; Ward *et al.*, 2000; Yoshioka *et al.*, 2000) and *in vivo* (Alonso *et al.*, 1990; English *et al.*, 1998; Hokama *et al.*, 2007; Jung *et al.*, 2010; Kameya *et al.*, 2009; Ogiso *et al.*, 1986, 1989; Padowski and Pollack, 2012; Torii *et al.*, 2001). While troubleshooting we determined that the rat hepatocyte matrix contained heptanoic acid at a high concentration (~1500 μM), a result confirmed by the manufacturer (BioIVT) as a means of increasing phase II metabolism. We hypothesized that the high concentration of heptanoic acid was saturating VPA and EHA metabolism, which is why no parent loss was observed. Removal of heptanoic acid from the *in vitro* test system resulted in significant parent loss (data not shown). Heptanoic acid-free medium [InVitroGRO KHB (heptanoic acid-free version)] was used in all subsequent metabolism experiments.

Rat hepatocytes were able to metabolize VPA, EHA, PHA, and HDA. The rate and extent of metabolism was higher for PHA and HDA relative to VPA and EHA. The calculated *in vitro* intrinsic clearance values for rat hepatocytes ranged from 5 μl/min/million cells for VPA to 89 μl/min/million cells for HDA and the overall rank order for intrinsic clearance was HDA > PHA > EHA > VPA. Intrinsic clearance in human hepatocytes followed the same rank ordering as rat hepatocytes; however, the rate of metabolism was about 1.5–6.5 folds lower.

PBPK modeling

The PBPK modeling approach is shown in Supplementary Figure 1. A similar modeling workflow was used for each of the 4 chemicals. For each chemical, a generic rat PBPK model (Supplementary Figure 2 and Supplementary Table 2) was used as the starting model and was parameterized with *in silico* estimates for chemical specific parameters. Results of the sensitivity analysis (Supplementary Table 3) identified oral permeability, hepatic metabolism, and plasma protein binding as the most sensitive biochemical parameters in the model and as such *in silico* estimates were replaced with *in vitro* values. The final chemical specific parameters used in the PBPK models are shown in Supplementary Table 4.

The literature search for existing oral PK rat data identified 11 PK data sets for VPA and 1 for EHA (Supplementary Table 5). There was high variability in the PK data for VPA between studies administering the same oral dose, and there was not always a proportional increase in internal exposure between studies with increasing doses (Supplementary Figure 3). This 'noise' in the data is important to keep in mind when reviewing the results of the PBPK model for VPA and the model should not be expected to be more accurate than the existing *in vivo* data. Comparison of model simulations to *in vivo* PK data is summarized in Figures 4 and 5 and Supplementary Figure 4 and Supplementary Table 6. The PBPK models for VPA and EHA provided good estimates of Cmax as illustrated by Cmax ratios (simulated vs observed) ranging from 0.29 to 1.96. Since enterohepatic recirculation occurs for these compounds *in vivo* but was purposely not included in the PBPK model structure, 2-time ranges (before recirculation: 0–3 h; including recirculation: 0 to end of study) were used to evaluate the shape of the plasma versus time curve and plasma AUC. The AUC_{0-3h} ratios (predicted vs observed) for VPA ranged from 0.21 to 2.52 and for EHA was 0.18. The reported data for EHA was based on measured total radioactivity in plasma and is not specific to the parent chemical and as such, it is not surprising that the model underpredicts AUC. To establish oral equivalent doses for VPA, EHA, PHA, and HDA, the PBPK model for VPA was first used to estimate the Cmax in plasma (the relevant dose metric for toxicity; Nau, 1986) associated with the oral NOAEL (150 mg/kg/day). The resulting plasma Cmax for VPA in rat following an oral dose of 150 mg/kg/day was 128 μg/ml. The plasma concentration of 128 μg/ml was then set as the target internal exposure metric for EHA, PHA, and HDA. The results of these simulations are summarized in Figure 6 and the oral equivalent doses were 150 mg/kg (VPA), 228 mg/kg (EHA), 516 mg/kg (PHA), and 1120 mg/kg (HDA).

DISCUSSION

In order to assess the biological activity similarity among a series of branched carboxylic acids, we evaluated the changes in gene expression elicited by these branched carboxylic acids. The patterns of gene expression for EHA and PNA were highly correlated to that for VPA, which we used as an anchor chemical in evaluating the series. The gene expression patterns for the rest of the chemicals we tested were not well correlated with VPA, indicating that they had different targets, and that read-across between these and VPA is inappropriate even though these chemicals have similar structural features to the VPA. When compared to all chemicals and other perturbations in a large gene expression database using the same experimental protocol, VPA, EHA, and PNA all displayed strong connections to HDAC inhibitors, including entinostat, droxinostat, apicidin, and others (Figure 2). VPA is a recognized HDAC inhibitor (Göttlicher *et al.*, 2001; Krämer *et al.*, 2003) and HDAC inhibition appears to be responsible for VPA's developmental toxicity (Eikel *et al.*, 2006; Go *et al.*, 2011; Göttlicher *et al.*, 2001; Jergil *et al.*, 2011; Metruccio *et al.*, 2020; Paradis and Hales, 2015; Parodi *et al.*, 2021; Wiltse, 2005). Molecular docking

Downloaded from https://academic.oup.com/toxsci/article/191/2/343/6965632 by guest on 24 September 2025

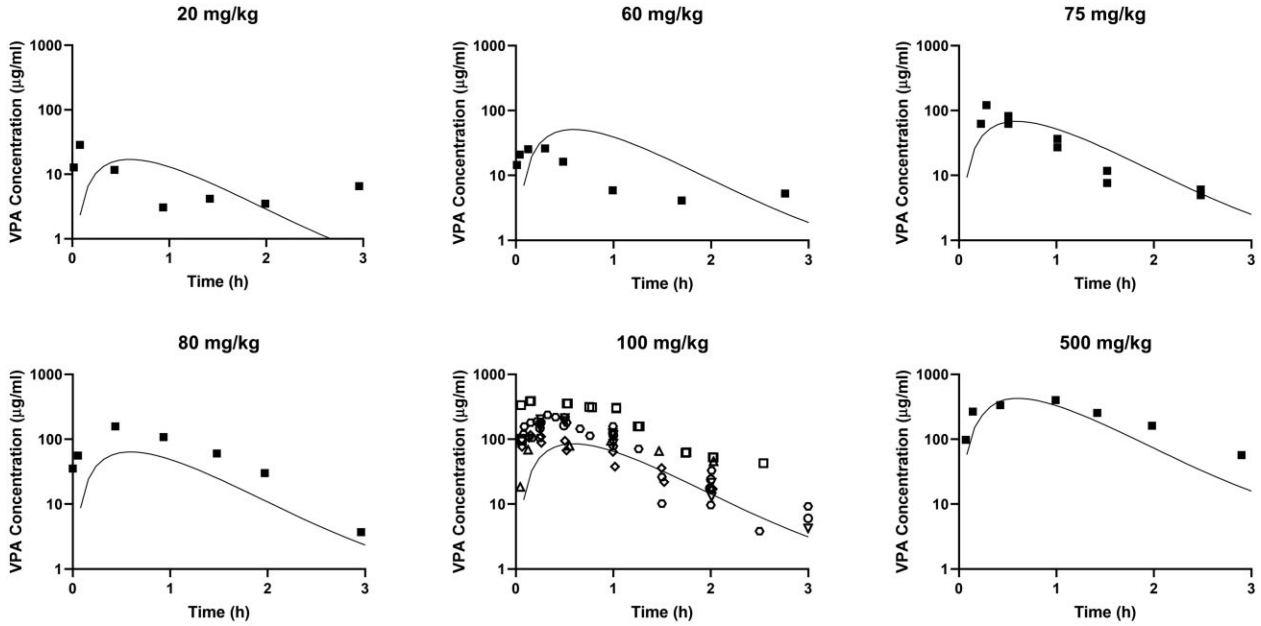

Figure 4. Plasma concentration (µg/ml) versus time (h) simulations (lines) from VPA PBPK model and PK data (symbols). References for PK data sets are provided in Supplementary Table 5.

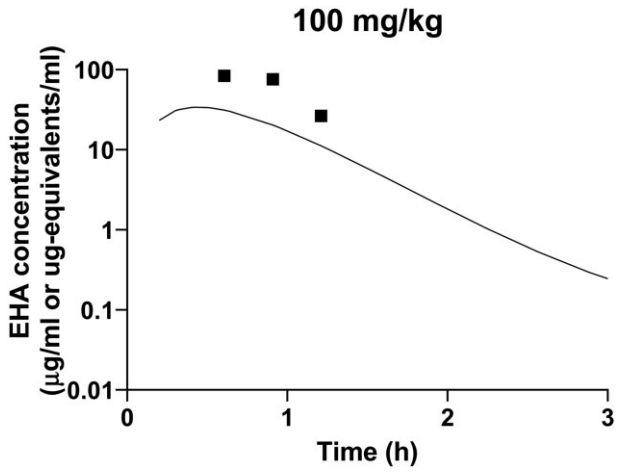

Figure 5. Plasma concentration (µg/ml or µg-equivalents/ml) versus time (h) simulations (lines) from EHA PBPK model and PK data (symbols). Experimental data expressed as microgram equivalents of EHA following oral exposure to [2-^{14}C-hexyl] EHA and simulations expressed as microgram EHA. PK data obtained from English *et al.* (1998).

simulations as shown in Figure 3 provided a basis for understanding how VPA, EHA and PNA were able to interact with HDAC (specifically with HDAC1, 3, and 8), whereas carboxylic acids with longer or shorter chains did not.

Acids with shorter branched alkyl chains such as both R, R_1 < C3 in Figure 7A (EBA), with longer branched alkyl chains such as R, R_1 > C4 in Figure 7B (PHA and HAD), or with alkyl chain R < C2, R_1 < C8 in Figure 7C (MNA) do not elicit the same gene expression pattern as VPA and EHA. None of the compounds in Figure 7A–C appear to be HDAC inhibitors based on gene expression results and the docking model exercise. However, acids with branched alkyl chains C1 < R < C5, C2 < R_1 < C8 in Figure 7D, including VPA, EHA, and PNA, have the potential to bind with and inhibit HDACs. This pattern is consistent with *in vivo* studies in which VPA, EHA, and PHA caused developmental toxicity in rodents, but other aliphatic acids did not (Di Carlo *et al.*, 1986; Narotsky *et al.*, 1994).

The use of transcriptomics as a tool for identifying modes of action and connections between treatments is attractive because chemical perturbation almost always results in changes in gene expression. However, given that no single cell type expresses the entire genome, the challenge in using transcriptomics for predictive toxicology is in choosing a panel of cell types that provides wide coverage of gene expression. Previous studies from our lab have shown that a carefully chosen panel of 4–6 cell types is sufficient to detect gene expression changes for hundreds of diverse chemicals (De Abrew *et al.*, 2019), and the LINCS study has resulted in gene expression signatures for more than 10 000 chemical and biological perturbations using a limited number of cell types (Subramanian *et al.*, 2017). One reason for conducting the present study was to determine whether a panel of cell types that are not undergoing an active developmental program (with the exception of the iPS-derived cardiomyocytes) could detect gene expression changes induced by a developmental toxicant. We conclude that the panel was sufficient in this instance. This could be attributable to the fact that the mode of action for VPA and its closely related analogs is not specific to development; however, to the extent that modes of developmental toxicity are known, molecular targets are not restricted to in their expression to just the embryonic stage (Wu *et al.*, 2013). Further research to evaluate gene expression for other developmental modes of action, as well as further cataloging of developmental modes of action will provide more confidence in using a finite number of cell types for nontargeted gene expression analysis.

Another aim of this study was to use PBPK modeling to make the read-across exercise quantitative; that is, to be able to use the VPA NOAEL to estimate the NOAELs for analogs with the same mode of action. The current work estimated the internal exposure (Cmax) associated with the rat oral developmental NOAEL for VPA (150 mg/kg/day) so that the Cmax (128 µg/ml) could be used as the target internal exposure for oral equivalent dose calculations. The PBPK models for EHA, PHA and HDA were then

Downloaded from https://academic.oup.com/toxsci/article/191/2/343/6965632 by guest on 24 September 2025

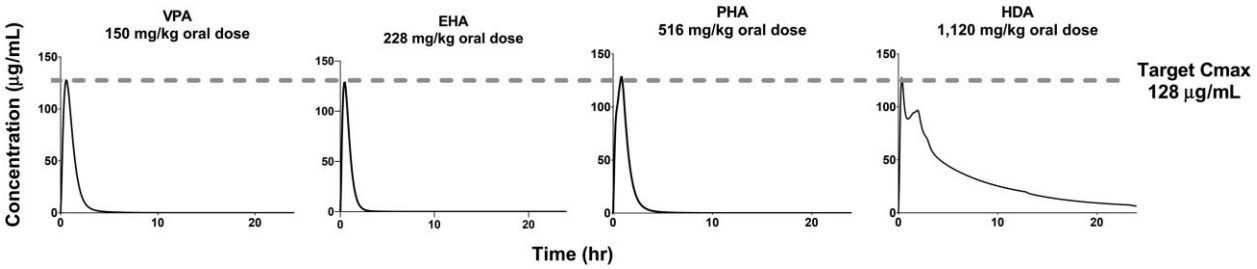

Figure 6. PBPK model simulation of plasma concentration (μg/ml) versus time (h) for rat oral equivalent dose based on plasma Cmax. The PBPK model for VPA was used to model the oral NOAEL (150 mg/kg) for VPA to establish the associated plasma Cmax (128 μg/ml) and set that as the target Cmax for EHA, PHA, and HDA.

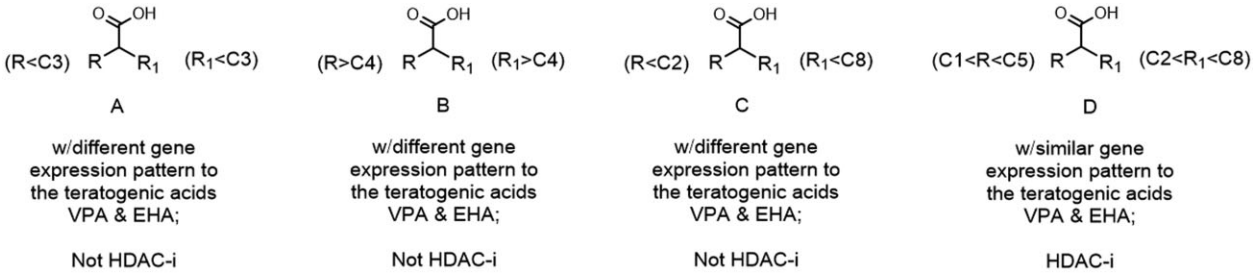

Figure 7. SAR structural patterns (A–D).

utilized for reverse dosimetry estimations to determine the oral dose that would result in the target Cmax (128 μg/ml). Only EHA has existing *in vivo* toxicity data that can be compared to the estimated oral equivalent dose from the PBPK model. In a well-designed prenatal oral developmental toxicity study in rats, EHA was orally gavaged at doses of 0, 100, 250, and 500 mg/kg/day from gestation day 6 to 15 (Hendrickx *et al.*, 1993). Significant reduction in fetal body weights and a significant increase in incidence of visceral malformation were observed in fetuses at the high dose. Reduction in fetal skeletal ossification was observed at the mid and high doses. As a result, the LOAEL and NOAEL for developmental toxicity were established at 250 and 100 mg/kg/day, respectively. The oral equivalent estimate from the PBPK model for EHA was 228 mg/kg which is in good agreement with the *in vivo* toxicity data.

In vitro metabolism of VPA, EHA, PHA, and HDA was determined using rat and human hepatocytes. The rank order for intrinsic clearance rate was the same between rat and human hepatocytes and followed: HDA > PHA > EHA > VPA. The rates of *in vitro* metabolism were faster for rat hepatocytes than human hepatocytes, which is consistent with the existing *in vivo* PK data for VPA (Löscher, 1978; Nau, 1986). When VPA was incubated with human hepatocytes, the rate and extent of parent chemical disappearances was essentially zero using the current assay conditions, which is consistent with other *in vitro* studies investigating the metabolism of VPA by human hepatocytes (Pradeep *et al.*, 2020). The low human hepatic metabolism of VPA is also observed *in vivo* where human PK data indicate a hepatic extraction ratio of 1% and plasma half-life of 16 h. Overall, the capacity of rats and humans to metabolize the current test compounds is anticipated to be well characterized by the current *in vitro* metabolism data given the consistency in the data for VPA.

The estimates from the PBPK model focused on concentration of VPA, EHA, PHA, and HDA in the plasma of adult rats whereas the endpoint of interest was developmental toxicity. Adult plasma concentrations represent fetal exposures. Multiple studies have investigated the relationship between the concentrations of VPA in maternal plasma versus concentration at the fetus. Studies examining the concentration of VPA in humans (Nau and Scott, 1984) or rats (Kobayashi *et al.*, 1990) demonstrated that the free (active) concentration of VPA was approximately equal or lower in the fetus relative to maternal concentrations. Some studies (Nau and Scott, 1986; Scott *et al.*, 1994) have reported that the concentration of VPA can be higher in the fetus, however, these comparisons were based on free (active) maternal concentration versus total (active + inactive) fetal concentration. The free concentration is the relevant concentration for toxicity mediated by VPA, and while the fetus may have a higher total concentration than maternal, more of the concentration is protein bound, thus resulting in lower free concentration relative to maternal (Nau *et al.*, 1984). Similar results for maternal versus fetal exposures have been reported for EHA (Nau *et al.*, 1984). As summarized by Nau (1992), transplacental PK is determined by various parameters. The rate of transfer depends on lipid solubility and the relative molecular mass of the chemical as well as on placental blood flow and structure, while the extent of transfer depends on protein binding of the chemical on each side of the placenta, active transport mechanisms, the presence of "deep compartments," and the degree of chemical ionization—with the degree of ionization being the most important parameter for acids (Nau, 1992). The higher lipid solubility of PHA and HDA compared to VPA and EHA, could in theory result in an increased rate of transfer across the placenta; however, this may be [partially or fully] offset by the higher molecular weight of PHA and HDA. Plasma protein binding is higher for PHA and HDA relative to VPA and EHA which would result in a lower free concentration for PHA and HDA to transfer across the placenta. The pKa values of the chemicals are similar. Overall, it is reasonable to assume that the relationship between maternal and fetal concentrations for PHA and HDA would be similar to VPA and EHA, that is, fetal free concentration is about equal to or lower than the free maternal concentration.

Downloaded from https://academic.oup.com/toxsci/article/191/2/343/6965632 by guest on 24 September 2025

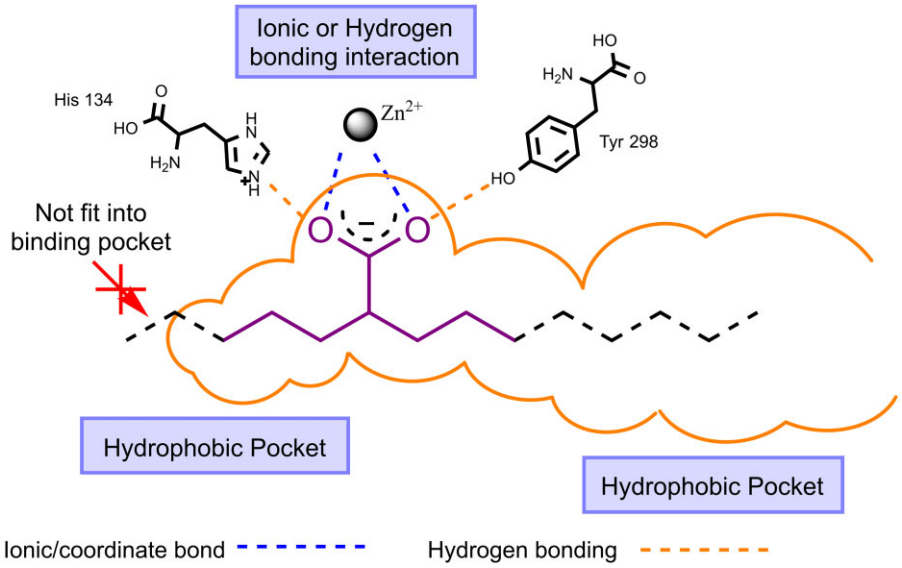

Figure 8. The binding pockets and interactions of HDAC enzyme with branched alkyl acids.

Docking experiments revealed that the binding pocket of HDAC contains 2 asymmetric hydrophobic pockets: a small one which can fit <C5 alkyl chain length and a larger one which accommodates longer chain length (Figure 8), indicating the importance of the length of branched alkyl chains. They may serve as an "anchor" within a hydrophobic pocket that facilitates ionic bonding (eg, Zn^{+}) or H-bonding (eg, Tyr 298 and His 134) interaction of acid group (Abouzeid *et al.*, 2007; Bermúdez-Lugo *et al.*, 2012; Bojic *et al.*, 1998). The molecular docking results demonstrate that VPA, EHA, and PNA fit well in the binding pocket of HDAC3 and have good binding via a C2-C3 R group as well as a $C \geq 3$ R_1 group, while the other branched carboxylic acids do not. These results provide additional means of understanding the gene expression results of the entire set and further support the conclusion that VPA is a suitable analog for some of the branched carboxylic acids but not others.

In summary, the structure activity relationship evaluation indicated that alkyl substituents R and R_1 (ie, C1 < R < C5 and C3 < R_1 < C8) at the alpha position of the carboxylic acid, including VPA, EHA, and PNA, have a significant impact on teratogenicity. These chemicals elicit a similar gene expression pattern as well as HDAC inhibition activity. As the chain lengths decrease or increase, teratogenicity decrease and these chemicals elicit different transcriptional changes and do not fit well in the biding pocket and interact with HDAC in docking models. Methyl branched alkyl acids such as MNA and linear alkyl acids such as OA also have poor interaction with one of hydrophobic pockets that affected ionic bonding and H-bonding with HDAC in docking models. These 2 alkyl acids showed weak or no teratogenicity. Chemical specific ADME data can be integrated into PBPK models for VPA, EHA, PHA, and HDA to account for differences in PK between the chemicals and provide a refinement of the toxicity-based read-across assessment for these compounds. The PBPK modeling results indicated that the developmental toxicity of these chemicals appear to decrease as the branched chain increases. The results on oral equivalent dose also indicated that the longer chain compound HDA would likely be 7× less toxic than VPA due to differences in PK. Overall, this work expands our understanding of the biological activity of branched alkyl acids and demonstrates how gene expression analysis can improve read-across.

Supplementary data

Supplementary data are available at *Toxicological Sciences* online.

Funding

Cefic (The Conseil Européen des Fédérations de l'Industrie Chimique).

Declaration of conflicting interests

The author/authors declared no potential conflicts of interest with respect to the research, authorship, and/or publication of this article.

Acknowledgments

The authors would like to thank Dr. Nadira De Abrew for his helpful technical comments and suggestions.

References

Abouzeid, L. A., El-Mowafy, A., Eikel, D., Nan, H., and Elmazar, M. M. (2007). Computational characteristics of valproic acid binding to histone deacetylase. *Saudi Pharm. J.* **15**, 183–189.

Alonso, I. G., Lanao, J. M., Martin, M. I., Mateos, A., Dominguez-Gil Hurlé, A., and Fermoso, J. (1990). Influence of a single dose of ethanol on the kinetics of valproic acid in rats. *Drug Metab. Dispos.* **18**, 732–734.

Barnes, G. L., Jr, Mariani, B. D., and Tuan, R. S. (1996). Valproic acid-induced somite teratogenesis in the chick embryo: Relationship with Pax-1 gene expression. *Teratology* **54**, 93–102.

Barter, Z. E., Bayliss, M. K., Beaune, P. H., Boobis, A. R., Carlile, D. J., Edwards, R. J., Houston, J. B., Lake, B. G., Lipscomb, J. C., Pelkonen, O. R., *et al.* (2007). Scaling factors for the extrapolation of in vivo metabolic drug clearance from in vitro data: Reaching a

Downloaded from https://academic.oup.com/toxsci/article/191/2/343/6965632 by guest on 24 September 2025

consensus on values of human microsomal protein and hepatocellularity per gram of liver. *Curr. Drug Metab.* **8**, 33–45.

Bermúdez-Lugo, J. A., Perez-Gonzalez, O., Rosales-Hernández, M. C., Ilizaliturri-Flores, I., Trujillo-Ferrara, J., and Correa-Basurto, J. (2012). Exploration of the valproic acid binding site on histone deacetylase 8 using docking and molecular dynamic simulations. *J. Mol. Model.* **18**, 2301–2310.

Blackburn, K., Bjerke, D., Daston, G., Felter, S., Mahony, C., Naciff, J., Robison, S., and Wu, S. (2011). Case studies to test: A framework for using structural, reactivity, metabolic and physicochemical similarity to evaluate the suitability of analogs for SAR-based toxicological assessments. *Regul. Toxicol. Pharmcol.* **60**, 120–135.

Blackburn, K., and Stuard, S. (2014). A framework to facilitate consistent characterization of read across uncertainty. *Regul. Toxicol. Pharmcol.* **68**, 353–362.

Bojic, U., Ehlers, K., Ellerbeck, U., Bacon, C. L., O'Driscoll, E., O'Connell, C., Berezin, V., Kawa, A., Lepekhin, E., Bock, E., *et al.* (1998). Studies on the teratogen pharmacophore of valproic acid analogues: Evidence of interactions at a hydrophobic center. *Eur. J. Pharmacol.* **354**, 289–299.

Chang, W., Cheng, J., Allaire, J. J., Sievert, C., Schloerke, B., Xie, Y., Allen, J., McPherson, J., Dipert, A., and Borges, B. (2021). *shiny: Web Application Framework for* R. R package version 1.7.1. Available at: https://CRAN.R-project.org/package=shiny.

De Abrew, K. N., Kainkaryam, R. M., Shan, Y. K., Overmann, G. J., Settivari, R. S., Wang, X., Xu, J., Adams, R. L., Tiesman, J. P., Carney, E. W., *et al.* (2016). Grouping 34 chemicals based on mode of action using connectivity mapping. *Toxicol. Sci.* **151**, 447–461.

De Abrew, K. N., Shan, Y. K., Wang, X., Krailler, J. M., Kainkaryam, R. M., Lester, C. C., Settivari, R. S., LeBaron, M. J., Naciff, J. M., and Daston, G. P. (2019). Use of connectivity mapping to support read across: A deeper dive using data from 186 chemicals, 19 cell lines and 2 case studies. *Toxicology* **423**, 84–94.

De Abrew, K. N., Overmann, G. J., Adams, R. L., Tiesman, J. P., Dunavent, J., Shan, Y. K., Carr, G. J., Daston, G. P., and Naciff, J. M. (2015). A novel transcriptomics based in vitro method to compare and predict hepatotoxicity based on mode of action. *Toxicology* **328**, 29–39.

Di Carlo, F. J., Bickart, P., and Auer, C. M. (1986). Structure metabolism relationships (SMR) for the prediction of health hazards by the environmental protection agency. II. Application to teratogenicity and other toxic effects caused by aliphatic acids. *Drug Metab. Rev.* **17**, 187–220.

Eikel, D., Lampen, A., and Nau, H. (2006). Teratogenic effects mediated by inhibition of histone deacetylases: Evidence from quantitative structure activity relationships of 20 valproic acid derivatives. *Chem. Res. Toxicol.* **19**, 272–278.

Ellison, C. A., and Wu, S. (2020). Application of structural and functional pharmacokinetic analogs for physiologically based pharmacokinetic model development and evaluation. *Regul. Toxicol. Pharmacol.* **114**, 104667.

English, J. C., Deisinger, P. J., and Guest, D. (1998). Metabolism of 2-ethylhexanoic acid administered orally or dermally to the female Fischer 344 rat. *Xenobiotica* **28**, 699–714.

Go, H. S., Seo, J. E., Kim, K. C., Han, S. M., Kim, P., Kang, Y. S., Han, S. H., Shin, C. Y., and Ko, K. H. (2011). Valproic acid inhibits neural progenitor cell death by activation of NF-κB signaling pathway and up-regulation of Bcl-XL. *J. Biomed. Sci.* **18**, 48.

Göttlicher, M., Minucci, S., Zhu, P., Krämer, O. H., Schimpf, A., Giavara, S., Sleeman, J. P., Lo Coco, F., Nervi, C., Pelicci, P. G., *et al.* (2001). Valproic acid defines a novel class of HDAC inhibitors inducing differentiation of transformed cells. *EMBO J.* **20**, 6969–6978.

Hamdoune, M., Duclos, S., Mounie, J., Santona, L., Lhuguenot, J. C., Magdalou, J., and Goudonnet, H. (1995). In vitro glucuronidation of peroxisomal proliferators: 2-ethylhexanoic acid enantiomers and their structural analogs. *Toxicol. Appl. Pharmacol.* **131**, 235–243.

Harrill, J. A., Everett, L. J., Haggard, D. E., Sheffield, T., Bundy, J. L., Willis, C. M., Thomas, R. S., Shah, I., and Judson, R. S. (2021). High-throughput transcriptomics platform for screening environmental chemicals. *Toxicol. Sci.* **181**, 68–89.

House, J. S., Grimm, F. A., Jima, D. D., Zhou, Y. H., Rusyn, I., and Wright, F. A. (2017). A pipeline for high-throughput concentration response modeling of gene expression for toxicogenomics. *Front. Genet.* **8**, 168.

Hendrickx, A. G., Peterson, P. E., Tyl, R. W., Fisher, L. C., Fosnight, L. J., Kubena, M. F., Vrbanic, M. A., and Katz, G. V. (1993). Assessment of the developmental toxicity of 2-ethylhexanoic acid in rats and rabbits. *Fundam. Appl. Toxicol.* **20**, 199–209.

Hokama, N., Hobara, N., Kameya, H., Ohshiro, S., Hobara, N., and Sakanashi, M. (2007). Investigation of low levels of plasma valproic acid concentration following simultaneous administration of sodium valproate and rizatriptan benzoate. *J. Pharm. Pharmacol.* **59**, 383–386.

International Programme on Chemical Safety (IPCS) (2010). *Characterization and Application of Physiologically Based Pharmacokinetic Models in Risk Assessment World Health Organization.* International Programme on Chemical Safety, Geneva, Switzerland.

Jergil, M., Forsberg, M., Salter, H., Stockling, K., Gustafson, A. L., Dencker, L., and Stigson, M. (2011). Short-time gene expression response to valproic acid and valproic acid analogs in mouse embryonic stem cells. *Toxicol. Sci.* **121**, 328–342.

Johannessen, C. U., and Johannessen, S. I. (2003). Valproate: Past, present, and future. *CNS Drug Rev.* **9**, 199–216.

Jung, B. H., Kim, B. J., Lee, M. S., Lee, J. H., Oh, J. H., and Lee, Y. J. (2010). Dose-dependent pharmacokinetics of toxic metabolites is not related to increased toxicity following high-dose valproic acid in rats. *J. Appl. Toxicol.* **30**, 775–778.

Kameya, H., Hokama, N., Hobara, N., Ohshiro, S., and Uno, T. (2009). Effects of a dopamine receptor agonist and atropine sulfate on absorption of valproic acid in rats. *Biomed. Res.* **30**, 101–106.

Kobayashi, S., Takai, K., Iga, T., and Hanano, M. (1990). Effect of pregnancy on the disposition of valproate in rats. *J. Pharmacobiodyn.* **13**, 533–542.

Krämer, O. H., Zhu, P., Ostendorff, H. P., Golebiewski, M., Tiefenbach, J., Peters, M. A., Brill, B., Groner, B., Bach, I., Heinzel, T., *et al.* (2003). The histone deacetylase inhibitor valproic acid selectively induces proteasomal degradation of HDAC2. *EMBO J.* **22**, 3411–3420.

Lamb, J., Crawford, E. D., Peck, D., Modell, J. W., Blat, I. C., Wrobel, M. J., Lerner, J., Brunet, J. P., Subramanian, A., Ross, K. N., *et al.* (2006). The Connectivity Map: Using gene-expression signatures to connect small molecules, genes, and disease. *Science* **313**, 1929–1935.

Lammer, E. J., Sever, L. E., and Oakley, G. P. Jr (1987). Teratogen update: Valproic acid. *Teratology* **35**, 465–473.

Löscher, W. (1978). Serum protein binding and pharmacokinetics of valproate in man, dog, rat and mouse. *J. Pharmacol. Exp. Ther.* **204**, 255–261.

Lennernäs, H. (2007). Intestinal permeability and its relevance for absorption and elimination. *Xenobiotica* **37**, 1015–1051.

Massa, V., Cabrera, R. M., Menegola, E., Giavini, E., and Finnell, R. H. (2005). Valproic acid-induced skeletal malformations: Associated gene expression cascades. *Pharmacogenet. Genomics* **15**, 787–800.

Downloaded from https://academic.oup.com/toxsci/article/191/2/343/6965632 by guest on 24 September 2025

Macritchie, K. A., Geddes, J. R., Scott, J., Haslam, D. R., and Goodwin, G. M. (2001). Valproic acid, valproate and divalproex in the maintenance treatment of bipolar disorder. *Cochrane Database Syst. Rev*. **3**, CD003196.

Menegola, E., Broccia, M. L., Nau, H., Prati, M., Ricolfi, R., and Giavini, E. (1996). Teratogenic effects of sodium valproate in mice and rats at midgestation and at term. *Teratog. Carcinog. Mutagen*. **16**, 97–108.

Metruccio, F., Palazzolo, L., Di Renzo, F., Battistoni, M., Menegola, E., Eberini, I., and Moretto, A. (2020). Development of an adverse outcome pathway for cranio-facial malformations: A contribution from in silico simulations and in vitro data. *Food Chem. Toxicol.* **140**, 111303.

Mitsopoulos, P., and Suntres, Z. E. (2010). Cytotoxicity and gene array analysis of alveolar epithelial A549 cells exposed to paraquat. *Chem. Biol. Interact*. **188**, 427–436.

Narotsky, M., Francis, E., and Kavlock, R. (1994). Developmental toxicity and structure-activity relationships of aliphatic acids, including dose–response assessment of valproic acid in mice and rats. *Fundam. Appl. Toxicol*. **22**, 251–265.

Nau, H. (1992). Pharmacokinetics and drug metabolism in the design and interpretation of developmental toxicity studies. In *Risk Assessment of Prenatally-Induced Adverse Health Effects* (D. Neubert, R. Kavlock, H. J. Merker and J. Klein, Eds.), Springer, Heidelberg. ISBN 978-3-642-77753-0.

Nau, H., and Scott, W. J. Jr (1986). Weak acids may act as teratogens by accumulating in the basic milieu of the early mammalian embryo. *Nature* **323**, 276–278.

Nau, H. (1986). Species differences in pharmacokinetics and drug teratogenesis. *Environ. Health Perspect*. **70**, 113–129. Erratum in: *Environ. Health Perspect.* (1988) **77** following 156.

Nau, H., Helge, H., and Luck, W. (1984). Valproic acid in the perinatal period: Decreased maternal serum protein binding results in fetal accumulation and neonatal displacement of the drug and some metabolites. *J. Pediatr*. **104**, 627–634.

Nuwaysir, E., Bittner, M., Trent, J., Barrett, J., and Afshari, C. (1999). Microarrays and toxicology: The advent of toxicogenomics. *Mol. Carcinog*. **24**, 153–159.

Obach, R. S. (1999). Prediction of human clearance of twenty-nine drugs from hepatic microsomal intrinsic clearance data: An examination of in vitro half-life approach and nonspecific binding to microsomes. *Drug Metab. Dispos*. **27**, 1350–1359.

Ogiso, T., Ito, Y., Iwaki, M., and Yamahata, T. (1986). Disposition and pharmacokinetics of valproic acid in rats. *Chem. Pharm. Bull. (Tokyo)* **34**, 2950–2956.

Ogiso, T., Ito, Y., Iwaki, M., Yoneda, I., and Horibe, Y. (1989). Effects of anticonvulsants on plasma levels and entero-hepatic circulation of valproic acid and on hepatic drug metabolizing enzyme activities in rats. *J. Pharmacobiodyn*. **12**, 255–263.

Ornoy, A. (2009). Valproic acid in pregnancy: How much are we endangering the embryo and fetus? *Reprod. Toxicol*. **28**, 1–10.

Padowski, J. M., and Pollack, G. M. (2012). Influence of enterohepatic recycling on the time course of brain-to-blood partitioning of valproic acid in rats. *Drug Metab. Dispos*. **40**, 1846–1853.

Paradis, F.-H., and Hales, B. (2015). The effects of class-specific histone deacetylase inhibitors on the development of limbs during organogenesis. *Toxicol. Sci*. **148**, 220–228.

Parodi, C., Di Fede, E., Peron, A., Viganò, I., Grazioli, P., Castiglioni, S., Finnell, R. H., Gervasini, C., Vignoli, A., and Massa, V. (2021). Chromatin imbalance as the vertex between fetal valproate syndrome and chromatinopathies. *Front. Cell Dev. Biol*. **9**, 654467.

Pennanen, S., Tuovinen, K., Huuskonen, H., and Komulainen, H. (1992). The developmental toxicity of 2-ethylhexanoic acid in Wistar rats. *Fundam. Appl. Toxicol*. **19**, 505–511.

Pollack, G. M., and Brouwer, K. L. (1991). Physiologic and metabolic influences on enterohepatic recirculation: Simulations based upon the disposition of valproic acid in the rat. *J. Pharmacokinet. Biopharm*. **19**, 189–225.

Pradeep, P., Patlewicz, G., Pearce, R., Wambaugh, J., Wetmore, B., and Judson, R. (2020). Using chemical structure information to develop predictive models for in vitro toxicokinetic parameters to inform high-throughput risk-assessment. *Comput. Toxicol*. **16**, 100136.

Ritchie, M. E., Phipson, B., Wu, D., Hu, Y., Law, C. W., Shi, W., and Smyth, G. K. (2015). limma powers differential expression analyses for RNA-sequencing and microarray studies. *Nucleic Acids Res*. **43**, e47.

Robert, E., Löfkvist, E., and Mauguiere, F. (1984). Valproate and spina bifida. *Lancet* **324**, 1392.

Schyman, P., Printz, R. L., Estes, S. K., O'Brien, T. P., Shiota, M., and Wallqvist, A. (2019). Assessing chemical-induced liver injury in vivo from in vitro gene expression data in the rat: The case of thioacetamide toxicity. *Front Genet* **26**, 1233.

Scott, W. J., Jr, Collins, M. D., and Nau, H. (1994). Pharmacokinetic determinants of embryotoxicity in rats associated with organic acids. *Environ. Health Perspect*. **102**, 97–101.

Subramanian, A., Narayan, R., Corsello, S. M., Peck, D. D., Natoli, T. E., Lu, X., Gould, J., Davis, J. F., Tubelli, A. A., Asiedu, J. K., *et al.* (2017). A next generation connectivity map: L1000 platform and the first 1,000,000 profiles. *Cell* **171**, 1437–1452.e17.

Torii, M., Takiguchi, Y., Saito, F., Izumi, M., and Yokota, M. (2001). Inhibition by carbapenem antibiotic imipenem of intestinal absorption of valproic acid in rats. *J. Pharm. Pharmacol*. **53**, 823–829.

Ward, E. S., Pollack, G. M., and Brouwer, K. L. (2000). Probenecid-associated alterations in valproic acid pharmacokinetics in rats: Can in vivo disposition of valproate glucuronide be predicted from in vitro formation data? *Drug Metab. Dispos*. **28**, 1433–1439.

Wiltse, J. (2005). Mode of action: Inhibition of histone deacetylase, altering WNT-dependent gene expression, and regulation of beta-catenin–developmental effects of valproic acid. *Crit. Rev. Toxicol*. **35**, 727–738.

Wu, S., Blackburn, K., Amburgey, J., Jaworska, J., and Federle, T. (2010). A framework for using structural, reactivity, metabolic and physicochemical similarity to evaluate the suitability of analogs for SAR-based toxicological assessments. *Regul. Toxicol. Pharmcol*. **56**, 67–81.

Wu, S., Fisher, J., Naciff, J., Laufersweiler, M., Lester, C., Daston, G., and Blackburn, K. (2013). Framework for identifying chemicals with structural features associated with the potential to act as developmental or reproductive toxicants. *Chem. Res. Toxicol*. **26**, 1840–1861.

Yoshioka, H., Ida, S., Yokota, M., Nishimoto, A., Shibata, S., Sugawara, A., and Takiguchi, Y. (2000). Effects of lithium on the pharmacokinetics of valproate in rats. *J. Pharm. Pharmacol*. **52**, 297–301.

Yoon, M., Nong, A., Clewell, H. J., 3rd, Taylor, M. D., Dorman, D. C., and Andersen, M. E. (2009). Evaluating placental transfer and tissue concentrations of manganese in the pregnant rat and fetuses after inhalation exposures with a PBPK model. *Toxicol. Sci*. **112**, 44–58.

Zeng, M., and Cao, H. (2018). Fast quantification of short chain fatty acids and ketone bodies by liquid chromatography-tandem mass spectrometry after facile derivatization coupled with liquid-liquid extraction. *J. Chromatogr. B* **1083**, 137–145.

Zhang, J. D., Berntenis, N., Roth, A., and Ebeling, M. (2014). Data mining reveals a network of early-response genes as a consensus signature of drug-induced in vitro and in vivo toxicity. *Pharmacogenomics J*. **14**, 208–216.

Downloaded from https://academic.oup.com/toxsci/article/191/2/343/6965632 by guest on 24 September 2025